Chains of atoms embedded into transition metal dichalcogenides as one-dimensional half-metallic magnets

Francis H. Davies [1,2] and Arkady V. Krasheninnikov [1]

[1] *Institute of Ion Beam Physics and Materials Research Helmholtz-Zentrum Dresden-Rossendorf 01328 Dresden, Germany*

[2] *Department of Physics, University of Exeter, Stocker Road, Exeter, EX4 4QL, United Kingdom*

(Received 30 January 2024; revised 8 April 2024; accepted 10 April 2024; published 30 April 2024)

Quasi-one-dimensional structures, single chains of Pt and Co atoms embedded into mirror twin boundaries in two-dimensional MoS_2, have recently been fabricated [Guo *et al.*, Nat. Synth. **1**, 245 (2022)]. Using both collinear and noncollinear first-principles calculations, we predict that other transition metals can form similar structures, and that these systems should possess exciting electronic and magnetic properties and specifically exhibit half-metallic electronic behavior. We further analyze the magnetocrystalline anisotropy of these systems and show that they possess unique easy axes and varying strengths of anisotropy, making thus efficient magnetization switching possible. We finally discuss the potentials of using single-atom chains embedded in MoS_2 and other transition metal dichalcogenides in spintronic devices.

DOI: 10.1103/PhysRevB.109.165442

I. INTRODUCTION

One-dimensional (1D) metallic nanostructures have garnered significant attention owing to their intriguing physical properties and potential applications in a multitude of fields. Specifically, these structures exhibit a rich tapestry of phenomena, including Peierls instability [1–5] and Tomonaga-Luttinger liquid (TLL) [6–10] or Majorana fermion [11,12] behavior due to their 1D nature and strong electron correlations, and also provide insights into other physical phenomena, such as size-quantization effects [13,14] and Aubry-type transitions [15]. They exhibit intriguing magnetic properties [16–19], which are of interest to the field of spintronics [20], where the giant magnetoresistance effect is commonly utilized [21–23]. Moreover, they possess versatile electronic characteristics [9–14,24], making the physics of these systems a fascinating area of research, driving a surge in exploration and experimentation in this domain.

The realization of 1D structures comes with tremendous challenges. Various approaches have been explored, including the creation of free-standing metal atom chains by mechanically breaking junctions between two leads [25–27], growth of chains by self-organization on substrates [13,28] or edges of two-dimensional (2D) materials [29], atomic manipulation [14,16,18], encapsulation inside carbon nanotubes[30–32], or even using cold trapped ions in optical lattices [15]. Each of these methods brings its own set of stabilization issues and considerations about the effects of encapsulation; see Ref. [33] for an overview. For example, carbon nanotubes [34] themselves may possess metallic properties, adding an additional layer of complexity to the study of 1D structures.

1D structures have also been implemented at the interfaces between two 2D materials, such as transition metal dichalcogenides (TMDs) [35], heterostrained bilayer graphene [36] by embedding boron nanostructures into graphene [37], or at the mirror twin boundaries (MTBs) in TMDs [8]. Moreover, recent experiments [38] also showed that 1D structures can be formed by embedding transition metal (TM) atoms into MTBs thus creating a single-metal-atom chain (SMAC). A chemical vapor codeposition technique was used to grow Pt SMACs at MTBs within a 2D MoS_2. The observed SMACs had an average length of up to 17 nm and showed excellent stability under ambient conditions. The Pt SMACs were found to exhibit metallic behavior and formed a network conduction pathway within the 2D film. The method was also successfully applied to Co SMACs, which gives rise to two questions: Can the method be extended to other TMs, and if yes, what magnetic and electronic properties will such SMACs have?

In this study, inspired by the findings of Guo *et al.* [38], we address these two questions. Using density functional theory (DFT) calculations we perform a systematic study of SMACs formed by 21 different TMs at MTBs in 2D MoS_2. To assess the likelihood of the experimental realization of SMACs, we calculate the energy of configurations when TM atoms are embedded into an MTB or basal plane of MoS_2. We further study the electronic structure and magnetic properties of all systems, using both collinear and noncollinear calculations. We find half-metallicity in a subset of systems and demonstrate the localization of magnetic states to the SMAC. Finally we calculate the magnetocrystalline anisotropy of these materials to evaluate their potentials for use in modern spintronic devices.

II. COMPUTATIONAL APPROACH

In our calculations, we used plane-wave DFT with an energy cutoff of 500 eV. The PBE functional [39] was employed together with the PAW pseudopotentials [40], as implemented in the Vienna *Ab initio* Simulation Package (VASP)[41]. Brillouin zone integration was performed using the Monkhorst-Pack grids [42], with 2D supercell structures maintaining a k-point density equivalent to the primitive cell

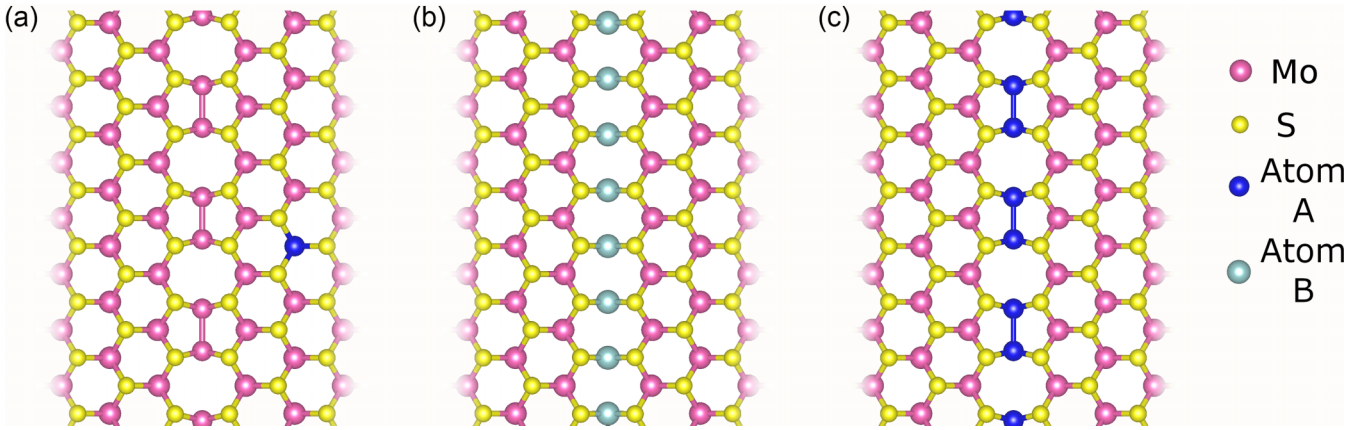

FIG. 1. Schematic representation of MoS_2 with an 8|55 MTB, both "naked" (a) and decorated with TM atoms substituting for Mo atoms (b, c). SMAC formed at the MTB can undergo dimerization or Peierls distortion, as illustrated in panel (c). A substitutional TM impurity in Mo atom position in the basal plan is shown in panel (a). The legend on the right displays the atomic species.

with an $8 \times 8 \times 1$ grid (or greater), and 1D structures maintaining a k-point density equivalent to $8 \times 1 \times 1$ (or greater). The supercells consisted of 130 atoms (two embedded TM atoms). Supercells of double sizes (four embedded TM atoms) were used in exchange interaction calculations. A vacuum gap of at least 15 Å was introduced to prevent spurious interactions with the system replicas. In the electronic/magnetic structure calculations we accounted for the spin-orbit coupling (SOC) [43] and also used the Hubbard+U approach [44]. As the choice of U can have a strong effect on the magnetic properties [45], while the exact value of this parameter is generally unknown, we investigated its influence on the results of calculations by considering a range of U values.

III. RESULTS AND DISCUSSION

A. Energetics of chains of transition metal atoms at mirror twin boundaries

To assess the likelihood of a SMAC forming at the MTB, we first calculated the energy gain or loss when replacing an infinite chain of Mo atoms, at the MTB, with the TM species, A (energy is per A atom). This configuration (referred to as C-sub, with "C" standing for "chain"), is compared to the case when the A atoms are incorporated into the basal plane of MoS_2 as substitutional impurities (referred to as B-sub, with "B" standing for "basal plane").

The formation energy of the C-sub configuration is given by

$$E_f[\text{C-sub}] = \tfrac{1}{2}E_{\text{MTB}}[\text{A}] + \mu_{\text{Mo}} - \tfrac{1}{2}E_{\text{MTB}} - \mu_{\text{A}}, \qquad (1)$$

where $E_{\text{MTB}}[\text{A}]$ represents the total energy of the system with a SMAC at the MTB normalized per A atom (note that we always used two atoms to account for possible dimerization of the chain; Fig. 1) and E_{MTB} represents the total energy of the system with a "naked" 8|55 MTB, which can also be referred to as Mo SMAC. We adopt standard notation of 8|55 to describe the morphology of MTB seen in Fig. 1(a) [46]. The symbols μ_{Mo} and μ_{A} denote the chemical potentials of Mo and the substitutional A atom, respectively. The formation energy of the B-sub configuration is given by

$$E_f[\text{B-sub}] = E_{\text{bulk}}[\text{A}] + \mu_{\text{Mo}} - E_{\text{bulk}} - \mu_{\text{A}}, \qquad (2)$$

where $E_{\text{bulk}}[\text{A}]$ is the total energy of the supercell with a substitutional atom A (in the position of Mo), as schematically illustrated in Fig. 1(a), and E_{bulk} is the energy of the pristine supercell.

We stress that although naked 8|55 MTBs have been observed in W-containing TMDs [47], they have not been found in MoS_2, as the naked 8|55 MTB has higher energy than MTBs of other types [46]. However, as as our goal is to assess the energy difference $\Delta E_f = E_f(\text{C-sub}) - E_f(\text{B-sub})$ for a wide range of TM atoms and compare it to ΔE_f for the structures with the experimentally realized elements [38] (Pt, Co), the choice of the MTB type and chemical potentials of the atoms is inconsequential resulting in only a uniform shift of all energies.

The atomic structure of a SMAC at MTB is illustrated in Figs. 1(b) and 1(c). The figure displays the MTB with impurity atoms substituting for Mo atom along the reflection line. Our calculations indicate that, as depicted in Fig. 1, there can be a noticeable dimerization of SMACs. The extent of dimerization varies for different TM atoms. For instance, elements such as Pt exhibit negligible atomic shifts, as shown in Fig. 1(b), while others, like Fe, show significant dimerization, which is related to the intricate effects related to band fillings (multiple bands cross E_F) and charge transfer from the edges, as discussed below.

The calculated formation energies of the C-sub and B-sub configurations for 21 SMACs are listed in Table S1 in the Supplemental Material [48], along with ΔE_f. The energy difference is presented in Fig. 2, which also indicates what structures have experimentally been realized [38].

Experimentally observed Pt SMACs have a calculated C-sub preferability of $\Delta E_f = 4.46$ eV, and Co has $\Delta E_f = 3.51$ eV, which serve as a point of comparison for other SMACs. Elements with greater favorability are expected to form SMACs more easily than Co, while those with lower favorability should be more challenging to form experimentally. Elements with negative values ΔE_f are expected not to form SMACs at all.

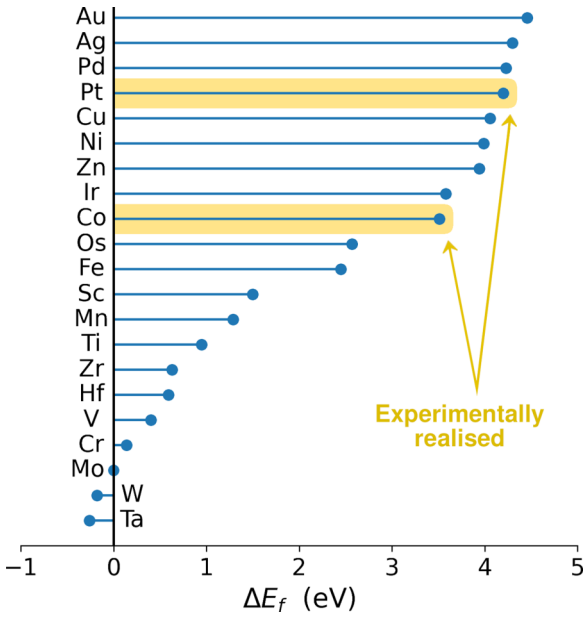

FIG. 2. A chart of ΔE_f, a comparison of the formation energy difference of C-sub and B-sub configurations for different elements. ΔE_f is positive when C-sub is energetically preferable and negative when B-sub is preferable. The energies are listed in order from most favorable to least favorable.

The data suggest that Pt is among the more favorable elements for SMAC formation, which is consistent with it being the first which was experimentally synthesized. Based on these energies, our results indicate that SMAC from other elements can also be realized. Specifically, it can be inferred that elements like Ir, Os, and Fe have the potential to form SMACs under comparable conditions.

B. Electronic structure of chains of transition metal atoms at mirror twin boundaries

Having optimized the geometry and assessed the energetics of SMACs at MTBs, we investigated the electronic structure and magnetic properties of 21 SMACs. Due to the symmetry of TMDs [49], it is not possible to construct a periodic supercell containing MTB (with or without SMAC), so that edges should be introduced. The presence of the edges gives rise to the states localized at the edges. This may give rise to a charge transfer from the edges to the MTB, as discussed previously [8,50]. The effects of the edges can be explored by calculating the electronic structure with different edge morphologies. We can then project the the states onto the atoms constituting the edge, the bulk, and the interface, allowing us to investigate this with two sulfur ion edges, single sulfur ion edges, and Mo ion edges.

This band projection is demonstrated in Fig. 3, where we use the bare MTB as a reference point, also here called the Mo SMAC. In this figure the electronic structure of the 8|55 MTB is presented for comparison. It showcases the projected states from different regions of the material. In Fig. 3(a), the simulated atomic structure is highlighted, with the edge, interface, and bulk regions displayed in distinct colors. The spin-split band structure around the Fermi level is depicted in Fig. 3(b), while the noncollinear electronic structure with spin-orbit coupling (SOC) is presented in Fig. 3(c).

The presence of SOC leads to band splitting in edge states, while the interface and bulk states remain unaffected. Although the bulk states maintain consistent dispersion across all substituting TMs, their position relative to the Fermi level varies. In contrast, the edge states display remarkable consistency, with a minor variation of only 0.04 eV across all systems. It is important to note that the interface states, influenced by SOC, vary depending on the specific interfacial TM element present.

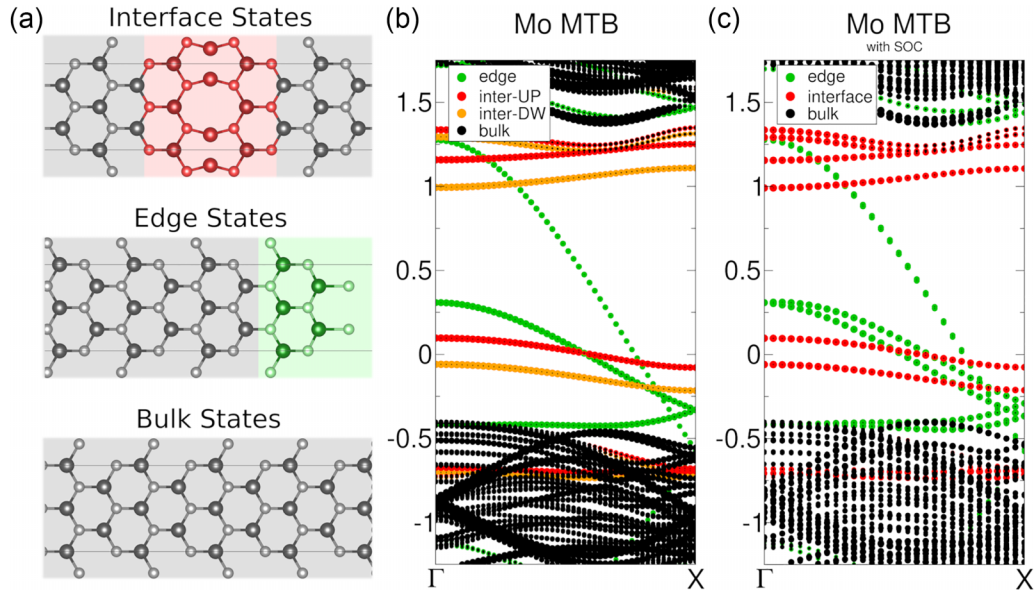

FIG. 3. Atomic and electronic structure of 8|55 MTB. (a) Highlighted/shaded regions schematically show the atoms used for edge, interface, and bulk projections. (b) Electronic bands associated with bulk (black), edge (green), and interface (red/gold) states calculated without SOC. (c) Electronic structure with account for noncollinear magnetism and SOC. Interface states shown in red only. Energies are in eV, and the Fermi level is set to zero.

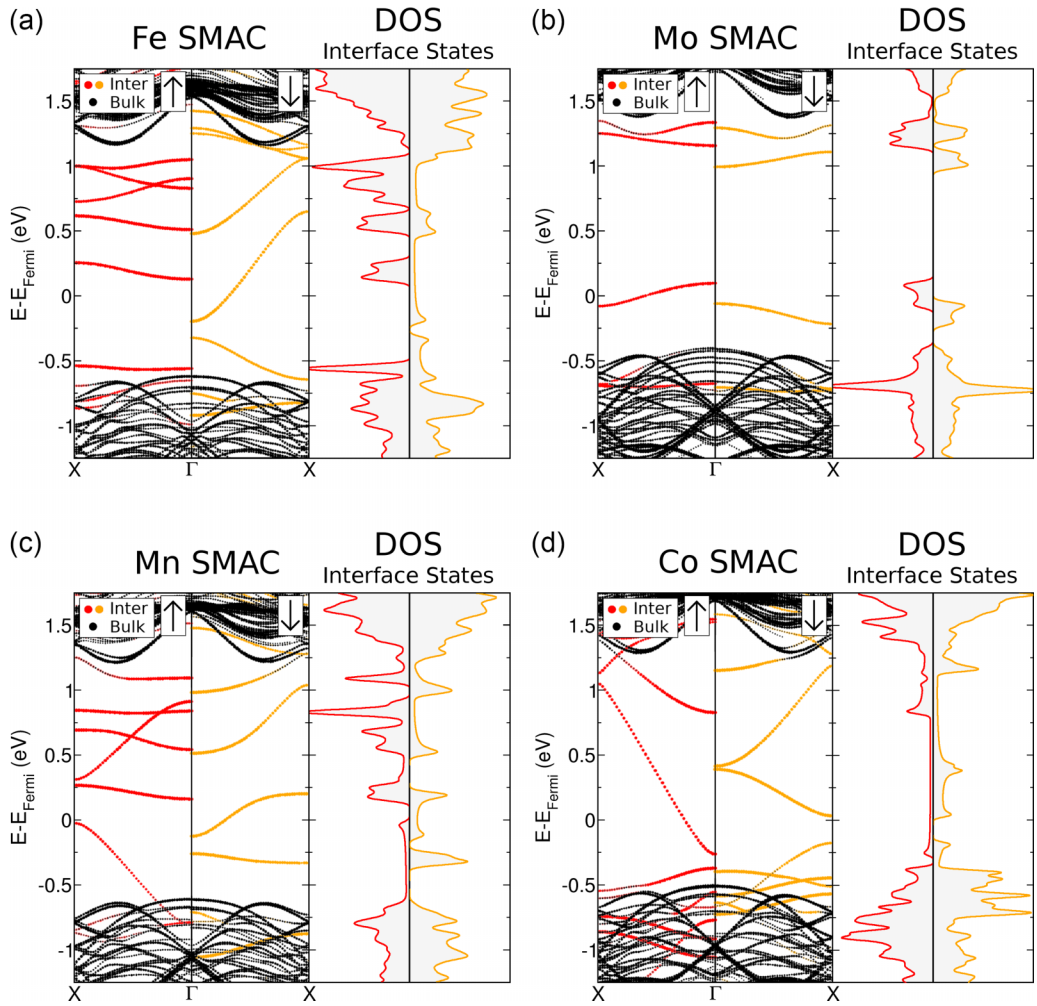

FIG. 4. Band structures for Fe, Mo, Mn, and Co SMACs. The bands associated with bulk states are plotted in black, edge states are omitted, and interface states are shown in red and gold for spin up and spin down, respectively.

Among the investigated SMACs with 21 TMs, six (Fe, Mn, W, Cr, Co, and Mo, with the last one corresponding to the naked 8|55 MTB) were found to exhibit half-metallic behavior, that is, the electronic structure in one spin channel is metallic, while there is a gap in the other, which is of considerable interest. Nevertheless, W and Cr are predicted to be among the least viable. As a result, we focus on the remaining four half-metallic SMACs, specifically the Fe, Mn, and Co SMACs. For the sake of comparison, we also present the results for Mo SMAC (8|55 MTB), as it does not involve any impurity atoms.

The band structures near the Fermi level of the four SMACs are presented in Fig. 4. These band structures show distinct electronic configurations for the two spin channels, emphasizing significant spin-dependent characteristics. Consequently, interface states attain full spin polarization within the band gap of the bulk states.

The Mo, Mn, and Co SMACs display metallic behavior in only one spin channel, with the Fermi level nearing a band associated with the other, nonmetallic spin channel. Applying a small gate voltage could enable a transition to fully spin-polarized conduction. In contrast, the Fe SMAC demonstrates distinct half-metallicity, featuring a region over 0.5 eV that shows complete spin polarization. This attribute significantly increases the potential of using Fe SMACs in spintronic applications.

We also investigated the role of the Hubbard term, and the results are shown in Fig. S1 [48]. By introducing the Hubbard parameter, the on-site Coulomb repulsion term within DFT calculations can be enhanced. This provides a corrective term to the DFT description of the electronic structure, especially in systems with transition metals, which have partially filled d orbitals and where electron correlation plays a significant role. The DFT+U approach helps to correct the shortcomings of standard DFT and has been shown to effect the magnetic character of materials including TMDs [45].

It is evident that accounting for U gives rise to very little disruption of the interface states. Here U is added to the interfacial atoms only, even in the case of the Mo MTB. As U increases from 0 to 6, energy shifts in bands occur gradually, rarely reaching 0.25 eV per increment in U. Moreover, the states have the potential to undergo subtle dispersion modifications while largely retaining their distinct configurations. In situations of considerable alteration, the

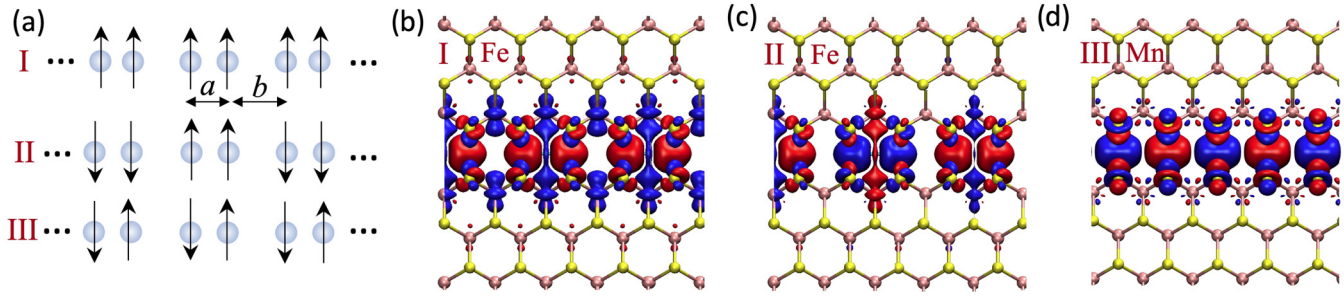

FIG. 5. Spin density in Mn, Fe, and Co chains embedded in an MTB in MoS_2. A supercell with four embedded TM atoms was used in the calculation. (a) Schematic illustration of spin orientations and Peierls distortion in the chains. (b, c) Spin density in a Fe chain, configurations I and II, respectively. Red and blue colors stand for majority/minority spin density. (d) AFM spin arrangement (configuration III) in Mn chain.

application of a gate voltage at the interface could effectively restore operational characteristics within a half-metallic segment of the band structure.

To examine the impact of edge states on the interface, we explored three distinct edges: the Mo edge, the 2S edge, and the 1S edge. Given the spatial separation between the edges and the interface, it is anticipated that they will not directly influence the interface bands. However, owing to charge transfer and Fermi level pinning, these states can undergo shifts possibly resulting in minor modifications.

The band structures presented in Fig. S2 [48] illustrate how the electronic states are influenced by the morphology of the edges. It can seen that the edge states are unique in each case; however, the interface bands remain largely unaffected. Figure S2(b), corresponding to the 1S edge, shows a modest shift in the interface bands, signifying a charge transfer to those states. Conversely, Fig. S2(c), representing the Mo edge, displays a negligible shift in the states. These observations are representative of Mo, Pt, Fe, and Co MTBs, despite the reconstruction of the edge, as can be seen in Fig. S3 [48]. Both the 1S edge and 2S edge states undergo band splitting due to SOC, while the Mo edge remains unaffected by SOC. Furthermore, although SOC affects the edge states in the case of the 1S edge and 2S edge, it does not impact the interface states, so that our results are robust with regard to the types of the edges.

C. Magnetic properties of single transition metal atom chains

As for the magnetic properties of SMACs, we concentrated on the three most interesting cases: Fe, Co, and Mn chains, which possess half-metal electronic structure and exhibit ferromagnetic behavior. The Mo chains, that is, the "naked" 8|55 MTBs, have higher energy in MoS_2 than MTBs of other types [46] and thus are unlikely to be manufactured. We carried out total energy calculations aimed at evaluating the exchange interactions for different spin configurations [Fig. 5(a)]. The spin densities and the energy differences are also presented in Fig. 5. We note that contrary to the free-standing chains of TM atoms [51], the periodicity in the atoms in the embedded chains is dictated by the matrix; that is, the sum of separations a and b always coincides with the unit cell size of MoS_2. For Fe and Co, the systems with strong Peierls distortion, we were unable to converge the system into AFM states when magnetic moments on the adjacent atoms pointed in opposite directions, as the separation between the atoms is small and FM interaction is very strong: instead, we always obtained a FM or nonmagnetic solution. In general, the convergence of the total energy for some spin configurations was challenging. This may also be related with the presence of metallic edge states interfering with the chain states (see Fig. 3), which created additional difficulties and required careful convergence of the results with respect to the number of k points: for some initial magnetic configurations spin density appeared at the edges, not at the chains of the embedded atoms. The energy differences between the configurations and magnetic moments on the embedded TM atoms are listed in Table I. Magnetic moments correlate with the number of unpaired f electrons. In these calculations, due to high computational costs, we did not account for magnetic anisotropy by including SOC. Our results can be used as input parameters for (semi) analytical models of magnetism in 1D systems [52–54], and specifically finite-length chains, where ferromagnetism was experimentally observed [19].

We also assessed magneto-crystalline anisotropy, as it plays a crucial role in determining a SMAC potential for spintronic applications. The anisotropy was evaluated by orienting the spin vector of the chain in different directions and calculating the interaction with the atomic orbitals. For this set of materials, the equation for the anisotropy can be expressed as [55]

$$\mathcal{E} = K_1 \sin^2\theta \cos^2\phi + K_2 \sin^2\theta \sin^2\phi + K_3 \cos^2\theta, \quad (3)$$

where $\mathcal{E}$ is the energy required to orientate the magnetic moment in a direction defined by, θ, the angel from the z axis and, ϕ, is the azimuthal angle in the x-y plain, originating from the x axis. The z axis is chosen to be normal to the plain of the 2D structure while the x axis is chosen to be along the interface

TABLE I. Atom separations a and b (see Fig. 5) and energy difference for various configurations (magnetic exchange interactions) in Mn, Fe, and Co chains embedded in an MTB in MoS_2. Magnetic moments M on the embedded TM atoms are also listed.

	a (Å)	b (Å)	$E_{\uparrow\uparrow\uparrow\uparrow}$ (eV)	$E_{\uparrow\uparrow\downarrow\downarrow}$ (eV)	$E_{\uparrow\downarrow\uparrow\downarrow}$ (eV)	M (μ_B)
Mn	3.178	3.189	0	+0.17	+0.52	2.857
Fe	2.401	3.966	0	+0.04	—	1.770
Co	3.038	3.329	0	+0.09	—	0.688

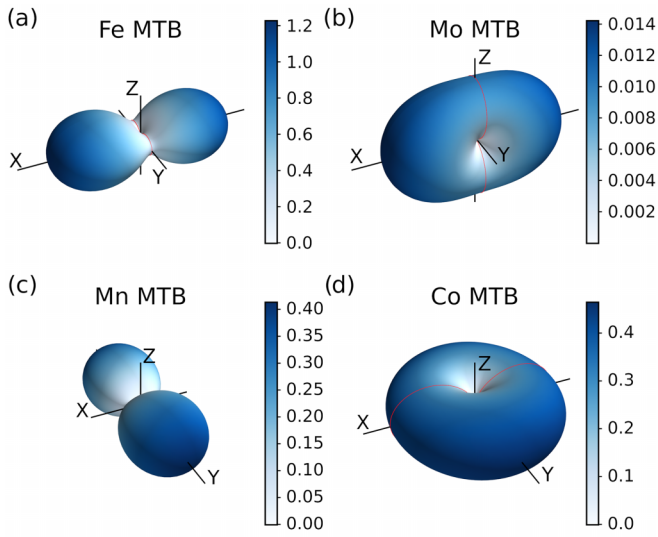

FIG. 6. Visualization of the free energy cost, in μeV, for the orientation of the magnetization vector as a three-dimensional energy surface. The distance from the origin to a point on the surface gives the anisotropy energy for magnetization in that direction of the crystal. The x axis is along the chain, the y axis is across the grain boundary, and the z axis is out of the plain.

direction. The coefficients K_1, K_2, and K_3 are derived from first-principles calculations. It is important to note that Eq. (3) describes relative energies, and as such, we set the energy of the easy axis to zero.

Figure 6 displays the magnetocrystalline anisotropy of Mo, Fe, Co, and Mn SMACs. Each of these materials exhibits a unique easy axis, demonstrating a lack of continuous spin symmetries. The anisotropy strength varies across different planes, leading to substantial differences in anisotropy energy along different directions, with the exception of the Co SMAC, which displays less variation. The anisotropy energy is smallest in the Mo chain with just 0.007 μeV/atom and largest for the Fe chain with 0.61 μeV/atom. Materials with low anisotropy such as these exhibit reduced preference for a specific magnetization direction. This makes it easier to align the magnetization in different directions, which can be advantageous for applications that require fast and efficient magnetization switching such as spin valves [56].

Low values of anisotropy energies may be beneficial or detrimental for using SMACs in spintronic devices. The low energies can easily lead to the breakdown of spin polarization, hindering device operation and leading to a reduction in magnetoresistance and a lower signal-to-noise ratio when reading domain-based data storage [56,57], thus necessitating the use of a pinning magnetic field.

However, in the case of spin valves, especially those used as sensors in read heads, maintaining complete spin polarization is not necessary. These devices depend on resistance variations caused by different magnetic orientations [56,58]. The advantage of a low anisotropy energy found for SMACs in this study is that it allows for quick and reversible changes in magnetization, improving the sensitivity and response time of these sensors, thereby enhancing their efficiency in reading data. Furthermore, given their small scale and the low energy required for reversibility, SMACs could be promising in the realm of spin logic devices [59]. In these devices, electron spins are utilized as an alternative to the traditional transistor-based logic, potentially offering a new approach to computational operations. The identified half-metallic SMACs, their electronic structures, and magnetocrystalline anisotropy provide opportunities for the development of reliable and accurate spintronic devices.

We note that, with regard to the MTB types, the 8|55 MTBs have the lowest formation energies [46] in W-based TMDs [47], hinting at a possibility to use a postsynthesis substitution (e.g., deposition of TM atoms on a system with MTBs combined with mild annealing) to create SMACs in W-based TMDs. Such structures must be much more robust and less sensitive to the effects of environment than free-standing chains or those created on the substrates.

IV. CONCLUSIONS

In conclusion, using first-principles calculations, we investigated 21 different TM elements forming SMACs embedded into MTBs in 2D MoS_2. By assessing their formation energies, and comparing the energies to those of the experimentally realized structures, we predict that growth of several SMACs in 2D MoS_2 and possibly other TMDs with unique properties should be feasible. In particular, the analysis of the electronic structure of Fe, Mo, Mn SMACs indicate that they should exhibit half-metallic electronic behavior. We also assessed magnetic exchange interactions in Mn, Fe, and Co chains. Our results can be used as input parameters for (semi) analytical models of magnetism in 1D systems [52–54], and specifically finite-length chains, where ferromagnetism was experimentally observed [19]. We also note that finite and relatively shot (tens of TM atoms) chains are expected to be realized in TMDs, as finite length MTBs exist either as chains across narrow flakes [8] or as triangles [60], so that studies on such systems can be interesting also in the context of 1D topological states [61,62]. We further analysed the magnetocrystalline anisotropy of these systems and show that they possess unique easy axes and varying strengths of anisotropy, making thus efficient magnetization switching possible and hinting at their possible applications in spintronics.

ACKNOWLEDGMENTS

We acknowledge funding from the German Research Foundation (DFG), project KR 4866/9-1 and the collaborative research center Chemistry of Synthetic 2D Materials CRC-1415-417590517. Generous CPU time grants from the Technical University of Dresden computing cluster (TAURUS) and Gauss Centre for Supercomputing e.V. and the Supercomputer HAWK at Höchstleistungsrechenzentrum Stuttgart are greatly appreciated. We further thank T. Michely, W. Jolie, A. Rosch, and A. Kakay for fruitful discussions.

[1] R. Peierls, *Quantum Theory of Solids* (Oxford University Press, London, 1955).

[2] H. W. Yeom, S. Takeda, E. Rotenberg, I. Matsuda, K. Horikoshi, J. Schaefer, C. M. Lee, S. D. Kevan, T. Ohta, T. Nagao, and S. Hasegawa, Instability and charge density wave of metallic quantum chains on a silicon surface, Phys. Rev. Lett. **82**, 4898 (1999).

[3] L. Wang, Y. Wu, Y. Yu, A. Chen, H. Li, W. Ren, S. Lu, S. Ding, H. Yang, Q.-K. Xue *et al.*, Direct observation of one-dimensional Peierls-type charge density wave in twin boundaries of monolayer $MoTe_2$, ACS Nano **14**, 8299 (2020).

[4] J. Deng, D. Huo, Y. Bai, X. Lin, Z. Cheng, and C. Zhang, Observations of charge-density-wave states in W_6Te_6 wires, Nano Lett. **23**, 7831 (2023).

[5] X. Yang, J.-J. Xian, G. Li, N. Nagaosa, W.-H. Zhang, L. Qin, Z.-M. Zhang, J.-T. Lü, and Y.-S. Fu, Possible phason-polaron effect on purely one-dimensional charge order of Mo_6Se_6 nanowires, Phys. Rev. X **10**, 031061 (2020).

[6] S.-i. Tomonaga, Remarks on Bloch's method of sound waves applied to many-fermion problems, Prog. Theor. Phys. **5**, 544 (1950).

[7] J. Luttinger, An exactly soluble model of a many-fermion system, J. Math. Phys. **4**, 1154 (1963).

[8] W. Jolie, C. Murray, P. S. Weiß, J. Hall, F. Portner, N. Atodiresei, A. V. Krasheninnikov, C. Busse, H.-P. Komsa, A. Rosch, and T. Michely, Tomonaga-Luttinger liquid in a box: Electrons confined within MoS_2 mirror-twin boundaries, Phys. Rev. X **9**, 011055 (2019).

[9] R. Stühler, F. Reis, T. Müller, T. Helbig, T. Schwemmer, R. Thomale, J. Schäfer, and R. Claessen, Tomonaga–Luttinger liquid in the edge channels of a quantum spin Hall insulator, Nat. Phys. **16**, 47 (2020).

[10] T. Zhu, W. Ruan, Y.-Q. Wang, H.-Z. Tsai, S. Wang, C. Zhang, T. Wang, F. Liou, K. Watanabe, T. Taniguchi *et al.*, Imaging gate-tunable Tomonaga–Luttinger liquids in ^{1}H-$MoSe_2$ mirror twin boundaries, Nat. Mater. **21**, 748 (2022).

[11] S. Nadj-Perge, I. K. Drozdov, J. Li, H. Chen, S. Jeon, J. Seo, A. H. MacDonald, B. A. Bernevig, and A. Yazdani, Observation of Majorana fermions in ferromagnetic atomic chains on a superconductor, Science **346**, 602 (2014).

[12] L. Schneider, P. Beck, J. Neuhaus-Steinmetz, L. Rózsa, T. Posske, J. Wiebe, and R. Wiesendanger, Precursors of Majorana modes and their length-dependent energy oscillations probed at both ends of atomic Shiba chains, Nat. Nanotechnol. **17**, 384 (2022).

[13] J. N. Crain and D. T. Pierce, End states in one-dimensional atom chains, Science **307**, 703 (2005).

[14] C. Chen, C. A. Bobisch, and W. Ho, Visualization of Fermi's golden rule through imaging of light emission from atomic silver chains, Science **325**, 981 (2009).

[15] A. Bylinskii, D. Gangloff, I. Counts, and V. Vuletić, Observation of Aubry-type transition in finite atom chains via friction, Nat. Mater. **15**, 717 (2016).

[16] D.-J. Choi, N. Lorente, J. Wiebe, K. von Bergmann, A. F. Otte, and A. J. Heinrich, Colloquium: Atomic spin chains on surfaces, Rev. Mod. Phys. **91**, 041001 (2019).

[17] M. Steinbrecher, R. Rausch, K. T. That, J. Hermenau, A. A. Khajetoorians, M. Potthoff, R. Wiesendanger, and J. Wiebe, Non-collinear spin states in bottom-up fabricated atomic chains, Nat. Commun. **9**, 2853 (2018).

[18] L. Schneider, P. Beck, T. Posske, D. Crawford, E. Mascot, S. Rachel, R. Wiesendanger, and J. Wiebe, Topological Shiba bands in artificial spin chains on superconductors, Nat. Phys. **17**, 943 (2021).

[19] P. Gambardella, A. Dallmeyer, K. Maiti, M. C. Malagoli, W. Eberhardt, K. Kern, and C. Carbone, Ferromagnetism in one-dimensional monatomic metal chains, Nature (London) **416**, 301 (2002).

[20] W. E. Pickett and H. Eschrig, Half metals: From formal theory to real material issues, J. Phys.: Condens. Matter **19**, 315203 (2007).

[21] M. N. Baibich, J. M. Broto, A. Fert, F. Nguyen Van Dau, F. Petroff, P. Etienne, G. Creuzet, A. Friederich, and J. Chazelas, Giant magnetoresistance of (001)Fe/(001)Cr magnetic superlattices, Phys. Rev. Lett. **61**, 2472 (1988).

[22] S. Parkin, X. Jiang, C. Kaiser, A. Panchula, K. Roche, and M. Samant, Magnetically engineered spintronic sensors and memory, Proc. IEEE **91**, 661 (2003).

[23] S. Pearton, D. Norton, R. Frazier, S. Han, C. Abernathy, and J. Zavada, Spintronics device concepts, IEE Proc. Circuits Devices Syst. **152**, 312 (2005).

[24] M. Liu, V. I. Artyukhov, and B. I. Yakobson, Mechanochemistry of one-dimensional boron: Structural and electronic transitions, J. Am. Chem. Soc. **139**, 2111 (2017).

[25] A. I. Yanson, G. R. Bollinger, H. E. van den Brom, N. Agraït, and J. M. van Ruitenbeek, Formation and manipulation of a metallic wire of single gold atoms, Nature (London) **395**, 783 (1998).

[26] A. Sokolov, C. Zhang, E. Y. Tsymbal, J. Redepenning, and B. Doudin, Quantized magnetoresistance in atomic-size contacts, Nat. Nanotechnol. **2**, 171 (2007).

[27] M. R. Calvo, J. Fernández-Rossier, J. J. Palacios, D. Jacob, D. Natelson, and C. Untiedt, The Kondo effect in ferromagnetic atomic contacts, Nature (London) **458**, 1150 (2009).

[28] P. C. Snijders and H. H. Weitering, Colloquium: Electronic instabilities in self-assembled atom wires, Rev. Mod. Phys. **82**, 307 (2010).

[29] K. Elibol, T. Susi, C. Mangler, D. Eder, J. C. Meyer, J. Kotakoski, R. G. Hobbs, P. A. van Aken, and B. C. Bayer, Linear indium atom chains at graphene edges, npj 2D Mater. Appl. **7**, 2 (2023).

[30] R. Senga, H.-P. Komsa, Z. Liu, K. Hirose-Takai, A. V. Krasheninnikov, and K. Suenaga, Atomic structure and dynamic behaviour of truly one-dimensional ionic chains inside carbon nanotubes, Nat. Mater. **13**, 1050 (2014).

[31] T. Fujimori, A. Morelos-Gómez, Z. Zhu, H. Muramatsu, R. Futamura, K. Urita, M. Terrones, T. Hayashi, M. Endo, S. Young Hong *et al.*, Conducting linear chains of sulphur inside carbon nanotubes, Nat. Commun. **4**, 2162 (2013).

[32] H.-P. Komsa, R. Senga, K. Suenaga, and A. V. Krasheninnikov, Structural distortions and charge density waves in iodine chains encapsulated inside carbon nanotubes, Nano Lett. **17**, 3694 (2017).

[33] M. Ma, S. Guo, X. Sang, C. Gao, Z. Liu, and Y. He, Structure, synthesis, and properties of single-metal-atom chains, Cell Rep. Phys. Sci. **3**, 101124 (2022).

[34] A. Jorio, G. Dresselhaus, and M. Dresselhaus, *Carbon Nanotubes: Advanced Topics in the Synthesis, Structure, Properties and Applications*, Topics in Applied Physics, Vol. 111 (Springer, Berlin, 2008).

[35] O. Ávalos-Ovando, D. Mastrogiuseppe, and S. E. Ulloa, Lateral heterostructures and one-dimensional interfaces in 2D transition metal dichalcogenides, J. Phys.: Condens. Matter **31**, 213001 (2019).

[36] G. R. Schleder, M. Pizzochero, and E. Kaxiras, One-dimensional Moiré physics and chemistry in heterostrained bilayer graphene, J. Phys. Chem. Lett. **14**, 8853 (2023).

[37] A. Quandt, C. Özdoğan, J. Kunstmann, and H. Fehske, Functionalizing graphene by embedded boron clusters, Nanotechnology **19**, 335707 (2008).

[38] S. Guo, J. Fu, P. Zhang, C. Zhu, H. Yao, M. Xu, B. An, X. Wang, B. Tang, Y. Deng *et al.*, Direct growth of single-metal-atom chains, Nat. Synth. **1**, 245 (2022).

[39] J. P. Perdew, K. Burke, and M. Ernzerhof, Generalized gradient approximation made simple; Phys. Rev. Lett. **77**, 3865 (1996).

[40] G. Kresse and D. Joubert, From ultrasoft pseudopotentials to the projector augmented-wave method, Phys. Rev. B **59**, 1758 (1999).

[41] G. Kresse and J. Furthmüller, Efficiency of *ab-initio* total energy calculations for metals and semiconductors using a plane-wave basis set, Comput. Mater. Sci. **6**, 15 (1996).

[42] J. D. Pack and H. J. Monkhorst, Special points for Brillonin-zone integrations, Phys. Rev. B **16**, 1748 (1977).

[43] S. Steiner, S. Khmelevskyi, M. Marsmann, and G. Kresse, Calculation of the magnetic anisotropy with projected-augmented-wave methodology and the case study of disordered $Fe_{1-x}Co_x$ alloys, Phys. Rev. B **93**, 224425 (2016).

[44] V. I. Anisimov, J. Zaanen, and O. K. Andersen, Band theory and Mott insulators: Hubbard *U* instead of Stoner *I*, Phys. Rev. B **44**, 943 (1991).

[45] E. R. Ylvisaker, W. E. Pickett, and K. Koepernik, Anisotropy and magnetism in the LSDA + U method, Phys. Rev. B **79**, 035103 (2009).

[46] H.-P. Komsa and A. V. Krasheninnikov, Engineering the electronic properties of two-dimensional transition metal dichalcogenides by introducing mirror twin boundaries, Adv. Electron. Mater. **3**, 1600468 (2017).

[47] Y.-C. Lin, T. Björkman, H.-P. Komsa, P.-Y. Teng, C.-H. Yeh, F.-S. Huang, K.-H. Lin, J. Jadczak, Y.-S. Huang, P.-W. Chiu, A. V. Krasheninnikov, and K. Suenaga, Three-fold rotational defects in two-dimensional transition metal dichalcogenides, Nat. Commun. **6**, 6736 (2015).

[48] See Supplemental Material at http://link.aps.org/supplemental/10.1103/PhysRevB.109.165442 for tabulated energetics of the embedded chains, dependence of the electronic structure on Hubbard parameter *U* and the influence of the edge states on the interface states.

[49] J. Ribeiro-Soares, R. M. Almeida, E. B. Barros, P. T. Araujo, M. S. Dresselhaus, L. G. Cançado, and A. Jorio, Group theory analysis of phonons in two-dimensional transition metal dichalcogenides, Phys. Rev. B **90**, 115438 (2014).

[50] C. Murray, C. van Efferen, W. Jolie, J. A. Fischer, J. Hall, A. Rosch, A. V. Krasheninnikov, H.-P. Komsa, and T. Michely, Band bending and valence band quantization at line defects in MoS_2, ACS Nano **14**, 9176 (2020).

[51] C. Ataca, S. Cahangirov, E. Durgun, Y.-R. Jang, and S. Ciraci, Structural, electronic, and magnetic properties of 3D transition metal monatomic chains: First-principles calculations, Phys. Rev. B **77**, 214413 (2008).

[52] S. Curilef, L. A. del Pino, and P. Orellana, Ferromagnetism in one dimension: Critical temperature, Phys. Rev. B **72**, 224410 (2005).

[53] Y. Xue, Z. Shen, Z. Wu, and C. Song, Theoretical prediction of Curie temperature in two-dimensional ferromagnetic monolayer, J. Appl. Phys. **132**, 053901 (2022).

[54] H. Xiang, C. Lee, H.-J. Koo, X. Gong, and M.-H. Whangbo, Magnetic properties and energy-mapping analysis, Dalton Trans. **42**, 823 (2013).

[55] L. D. Landau, E. M. Lifschitz, and L. P. Pitaevskii, *Electrodynamics of Continuous Media*, Course of Theoretical Physics Vol. 8, 2nd ed. (Pergamon Press, Oxford, 1984).

[56] M. Ashton, D. Gluhovic, S. B. Sinnott, J. Guo, D. A. Stewart, and R. G. Hennig, Two-dimensional intrinsic half-metals with large spin gaps, Nano Lett. **17**, 5251 (2017).

[57] W. Liu and Y. Xu, *Spintronic 2D Materials: Fundamentals and Applications* (Woodhead Publishing, 2019).

[58] D. Heim, R. Fontana, C. Tsang, V. Speriosu, B. Gurney, and M. Williams, Design and operation of spin valve sensors, IEEE Trans. Magn. **30**, 316 (1994).

[59] S. Manipatruni, D. E. Nikonov, C.-C. Lin, T. A. Gosavi, H. Liu, B. Prasad, Y.-L. Huang, E. Bonturim, R. Ramesh, and I. A. Young, Scalable energy-efficient magnetoelectric spin–orbit logic, Nature (London) **565**, 35 (2019).

[60] P. M. Coelho, H.-P. Komsa, H. Coy Diaz, Y. Ma, A. V. Krasheninnikov, and M. Batzill, Post-synthesis modifications of two-dimensional $MoSe_2$ or $MoTe_2$ by incorporation of excess metal atoms into the crystal structure, ACS Nano **12**, 3975 (2018).

[61] C. L. Fefferman, J. P. Lee-Thorp, and M. I. Weinstein, Topologically protected states in one-dimensional continuous systems and Dirac points, Proc. Natl. Acad. Sci. USA **111**, 8759 (2014).

[62] J. Zak, Symmetry criterion for surface states in solids, Phys. Rev. B **32**, 2218 (1985).